Supplementary Information

High-Performance PBI Membranes for Flow Batteries: From Transport Mechanism to Pilot Plant

Qing Dai[a,b], Feng Xing[a], Xiaonan Liu[a,b], Dingqin Shi[a], Congzhi Deng[a,b], Ziming Zhao[a,c,d] and Xianfeng Li[a,*]

[a] Division of Energy Storage, Dalian Institute of Chemical Physics, Chinese Academy of Sciences. 457 Zhongshan Road, Dalian, 116023 (P.R China).

[b] University of Chinese Academy of Sciences, Beijing, 100049 (P.R China).

[c] Changchun Institute of Applied Chemistry, Chinese Academy of Sciences, Changchun, 130022 (P.R China).

[d] University of Science and Technology of China, Hefei, 230026 (P.R China).

* Corresponding author. *E-mail address:* lixianfeng@dicp.ac.cn.

Experimental Section

The device and measuring method. Ion transport numbers (ITNs) were measured to determine the main charge carriers in PBI membrane. The experiment was performed with a concentration cell to determine the zero-current voltage (V_0) followed by treatment with Nernst relationship.[12,13] The device is an H-shape cell with two half cells separated by a sample membrane (Fig. S1a). Each half cell includes an electrode and a Luggin capillary (or an L-shape glass salt bridge), forming a four-electrode construction.[14] This configuration can avoid the influence of contact resistance and electrochemical polarization on electrodes so that the collected data can directly reflect the ion transport in solution and membrane phases. The I-V scan of the device was collected as the original data. As shown in Fig. S1b, the intercept on the abscissa is the zero-current potential, which is equal to the membrane potential of the concentration cell and can be treated by Nernst relationship to calculate the ITN (insert in Fig. 1b). The slope of the I-V line is the conductivity, whose reciprocal is the resistance between the tips of the two Luggin Capillaries.

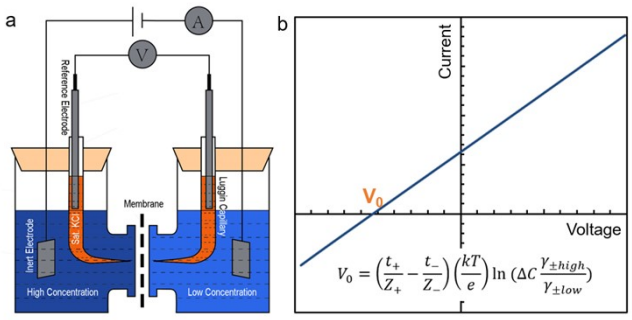

Fig. S1 Schematic diagram of the four-electrode cell (a) and the I-V line (b). V_0 is zero-current voltage. Insert is the Nernst relationship.

Preparation and treatment of PBI membrane. PBI polymer was synthesized following our previous work [1]. The membrane was prepared by evaporation of a casting solution. The membrane thickness is kept at 25±3 μm for lab-scale tests and 38±3 μm for stack.

Pristine PBI membranes were treated with different solutions by immersing in corresponding solutions overnight and washed with deionized water, named as X-PBI, where X represents the corresponding solutions including H_3PO_4 (85 wt.%), 3M H_2SO_4, 3M HCl, 3M NaOH, 3M KOH and 5.5M (~25 wt.%) KOH.

Ion transport number (ITN). The ion transport number was measured in a concentration cell by determining the zero-current voltage followed by treatment in Nernst relationship [2,3]. The device is an H-shape cell with two half cells separated by a membrane (Fig. 1a). The I-V curves of the device are collected with Gamry Interface 1000 or Reference 3000. The zero-current voltage of the I-V line was treated by Nernst relationship below, to calculate the ion transport number.

$$V_0 = \left(\frac{t_+}{Z_+} - \frac{t_-}{Z_-}\right)\left(\frac{kT}{e}\right) ln(\Delta C \frac{\gamma_{\pm high}}{\gamma_{\pm low}}) \quad (1)$$

Where V_0 is the zero-current voltage, t is the ion transport number, k is the Boltzmann constant, T is the Kelvin temperature, e is the elementary charge, C is the ratio of high concentration to the low concentration, $\gamma_{\pm high}$ and $\gamma_{\pm low}$ is the average activity coefficient in the high concentration solution and low concentration solution, respectively. Subscript "+" and "-" represent cation and anion, respectively.

Ion rectification. The pristine PBI membrane was assembled into a cell with one side filled with 1 M HCl and another side filled with 1 M KOH. Stand the cell while recording the membrane potential via OCV. The I-V linear scan was started after the membrane potential reaches equilibrium.

Area resistance and ion conductivity. The area resistance was tested in a H-type cell. The resistance was calculated from the slope of I-V line. The membrane resistance was calculated by the difference between the area resistance of devices with and without a membrane, following equation (2).

$$R_A = A(R_1 - R_2) \tag{2}$$

Where R_A is the area resistance, A is the effective area of membrane, and R_1 and R_2 are the device resistance with and without membrane, respectively.

The ion conductivity was calculated by the following equation.

$$\sigma = \frac{h}{R_A} \tag{3}$$

Where σ is the ion conductivity, h is the membrane thickness.

Ion selectivity. Membrane conductivity and ion transport number were tested in different solutions. The ion selectivity was calculated by the following equation.

$$S_{i/j} = \frac{\sigma_i}{\sigma_j} \tag{4}$$

Where $S_{i/j}$ is the ion selectivity of ion i over ion j, and σ_i and σ_j is the ion conductivity of ion i and ion j, respectively, which is calculated by the following equation.

$$\sigma_i = \frac{\sigma \times t_i}{z_i^2}$$

(5)

Where σ is the conductivity of the salt and t_i is the ITN of i, and z_i is the charge number of i.

Activation energy. The activation energy of the membrane was calculated from the ion conductivities at different temperatures. Arrhenius relationship was used to calculate the activation energy.

$$\sigma = \frac{\sigma_0}{T} exp(-\frac{E_a}{kT})$$

(6)

or in the logarithmic form:

$$\ln(\sigma T) = \ln(\sigma_{0\pm}) - \frac{eE_a}{kT}$$

(7)

Where σ is the ion conductivity, T is the Kelvin temperature, and E_a is the activation energy in the unit of eV.

Respective activation energy of cation and anion was tested in a concentration cell and calculated by the following equation [4]:

$$\ln(\sigma t_{\pm} T) = \ln(\sigma_{0\pm}) - \frac{eE_{a,\pm}}{kT}$$

(8)

Swelling ratio. Membranes were cut into 5x5 cm^2 pieces and equilibrated in different solutions. Then the area and weight were measured after wiping the solution on membrane surface. The area-based swelling ratio is:

$$SW_A = \frac{A_{swelling} - A_{dry}}{A_{dry}} \quad (9)$$

Where SW_A is the area-based swelling ratio, A_{dry} and $A_{swelling}$ is the area of membrane after and before swelling, respectively.

The weight-based swelling ratio is:

$$SW_W = \frac{W_{swelling} - W_{dry}}{W_{dry}} \quad (10)$$

Where SW_W is the weight-based swelling ratio, $W_{swelling}$ and W_{dry} is the weight of membrane after and before swelling, respectively.

Characterizations. X-ray photoelectron spectrometer (XPS) experiments were carried out on ESCALAB Xi+ (ThermoFisher), and the data was treated by Avantage. The peak position was corrected by shifting the C1s peak to 284.8 eV. Fourier Transform Infrared Spectroscopy (FT-IR) experiments were carried out on Nicolet iS50 (Thermo Fisher). Raman spectrums were achieved at Senterra (Bruker Optics) with a laser of 1064-nm wavenumber.

Electrochemical Impedance Spectroscopy (EIS). The EIS experiment was carried

out on Gamry 3000 electrochemical workstation. Single batteries with 3×3 cm^2 effective area were tested by galvanostatic method with current of 10 mA and frequency range of 10^6 ~ 1 Hz. The experiment used two-electrode configuration where the working electrode connect with the anode and the counter electrode connect with the cathode.

Battery performance. The single battery was assembled following our previous report[5]. The VFB single batteries have effective areas of 6×8 cm^2 and equipped with 60 mL 1.5 M vanadium ions and 3 M H_2SO_4. The alkaline Zn-Fe single batteries have effective areas of 3×3 cm^2 and equipped with 40 mL 0.4 M ZnO in 3.8 M NaOH and 0.8 M $Fe(CN)_4^{2-}$ in 3 M KOH. The 3 kW VFB stack is assembled with 25 units of 940 cm^2 for each and the electrolyte volume is 30 L. The 1 kW alkaline Zn-Fe stack is assembled with 10 units of 1000 cm^2 for each, and the electrolyte composition is 60 L 0.8 M $Fe(CN)_4^{2-}$ and 3 M KOH for anolyte, and 60 L 0.6M ZnO and 5.2 M NaOH for catholyte. The performance is tested with Arbin BT 2000 (5V, 20A) for single batteries and Arbin BT 2000 (50V, 200 A) for stacks.

The relationship between ITN and Donnan effect[2,6]

For a monovalent ion pair AX, the ITN determined by Donnan effect can be expressed by the following equation:

$$\bar{t}_A = \frac{\bar{u}_A\left(\sqrt{\bar{C}_R^2 + 4C_AC_X} + \bar{C}_R\right)}{\bar{u}_A\left(\sqrt{\bar{C}_R^2 + 4C_AC_X}\right) + \bar{u}_X\left(\sqrt{\bar{C}_R^2 + 4C_AC_X} - \bar{C}_R\right)} \tag{11}$$

$$\bar{t}_X = \frac{\bar{u}_X\left(\sqrt{\bar{C}_R^2 + 4C_AC_X} + \bar{C}_R\right)}{\bar{u}_A\left(\sqrt{\bar{C}_R^2 + 4C_AC_X}\right) + \bar{u}_X\left(\sqrt{\bar{C}_R^2 + 4C_AC_X} - \bar{C}_R\right)} \tag{12}$$

Where C represents the ion concentration in the solution, $\bar{C}$ represents the ion concentration in the membrane, and $\bar{C}_R$ is the concentration of ion exchange groups (or fixed charges) in the membrane, $\bar{t}$ represents the ion transport number in the membrane phase, and $\bar{u}$ represents ion mobility in the membrane phase.

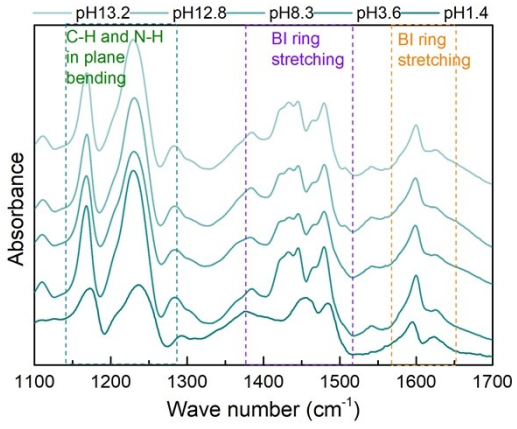

Fig. S2. The FT-IR spectrum of PBI membranes at different pH.

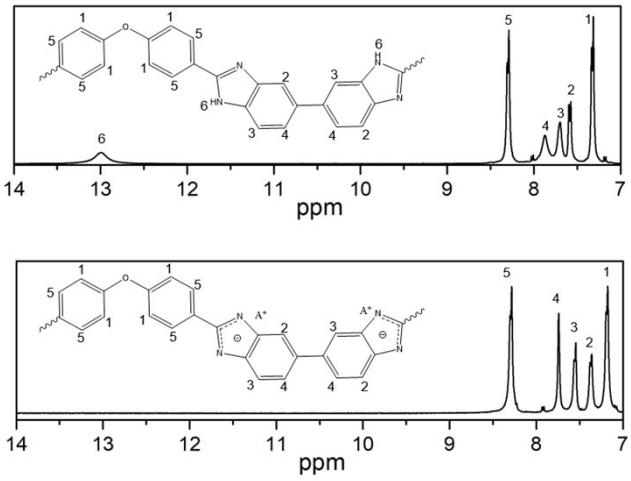

Fig. S3. The 1 H -NMR spectrum of the pristine PBI (top) and 3M KOH-PBI (bottom). After deprotonation, the chemical shift decreases because of the increase of screening effect at higher electronegativity.

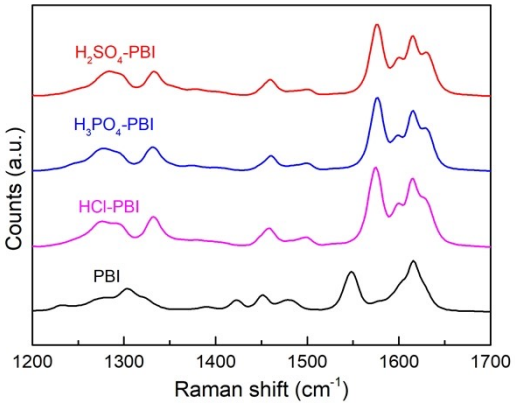

Fig. S4. The Raman spectrum of the pristine PBI membrane and PBI membranes treated with H_2SO_4, H_3PO_4 and HCl.

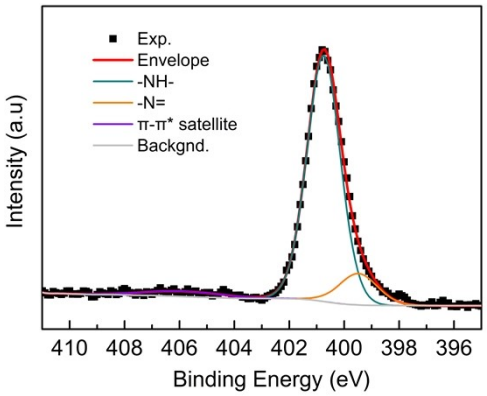

Fig. S5. The XPS spectrum of PBI membranes treated with 3M H_2SO_4.

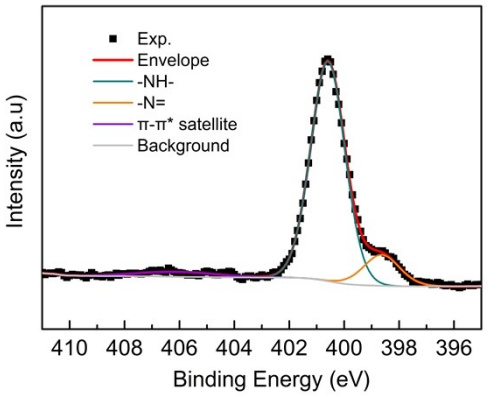

Fig. S6. The XPS spectrum of PBI membranes treated with H_3PO_4.

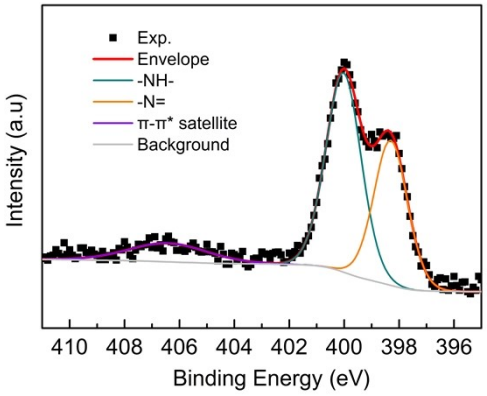

Fig. S7. The XPS spectrum of PBI membranes treated with 5.5M KOH.

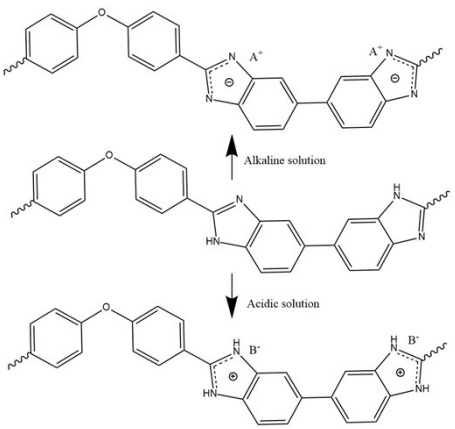

Fig. S8. The protonation and deprotonation of PBI in acidic and alkaline solutions, respectively.

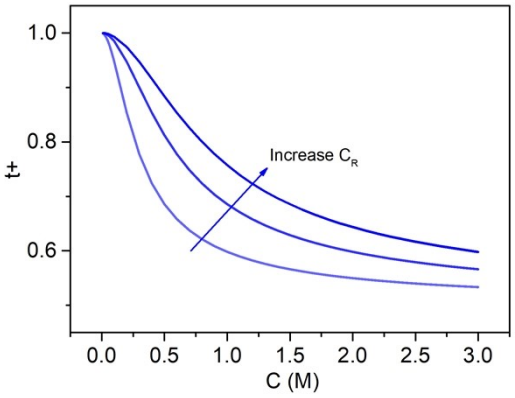

Fig. S9. The relationship of ion ITN with the solution concentration at different resident ion concentration in membrane simulated with Donnan membrane equilibrium (equation 11 and 12) [2,6]. Three lines are calculated by setting membrane fixed charge concentration (C_R) =0.4 0.8 and 1.2, respectively. The cation-anion mobility ratio (μ-/μ+) is set to 1.

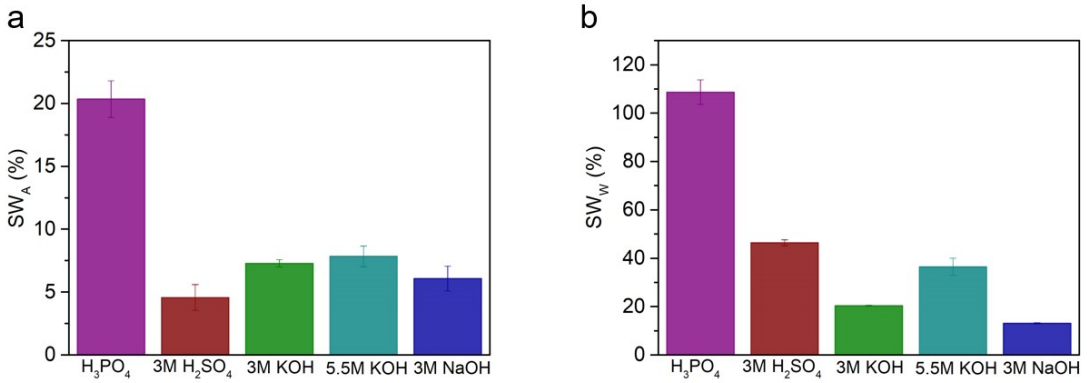

Fig. S10. The area-based swelling ratio (a) and weight-based swelling ratio (b) of PBI membranes in different solutions.

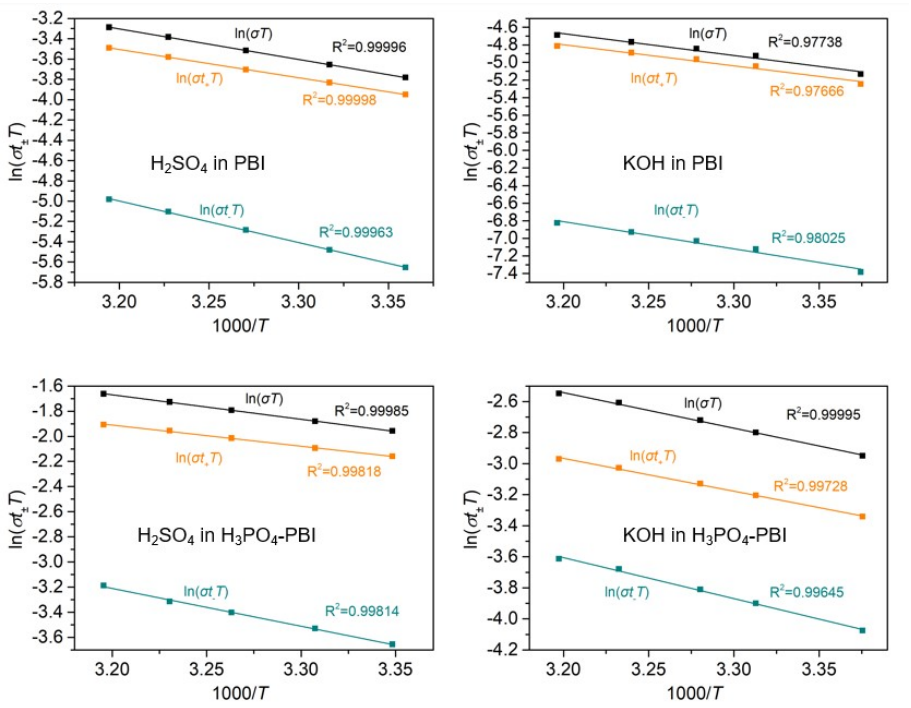

Fig. S11. The Arrhenius plot of ion transport in PBI or H_3PO_4-PBI. Cation: Orange; Anion: Dark Cyan; Total: Black.

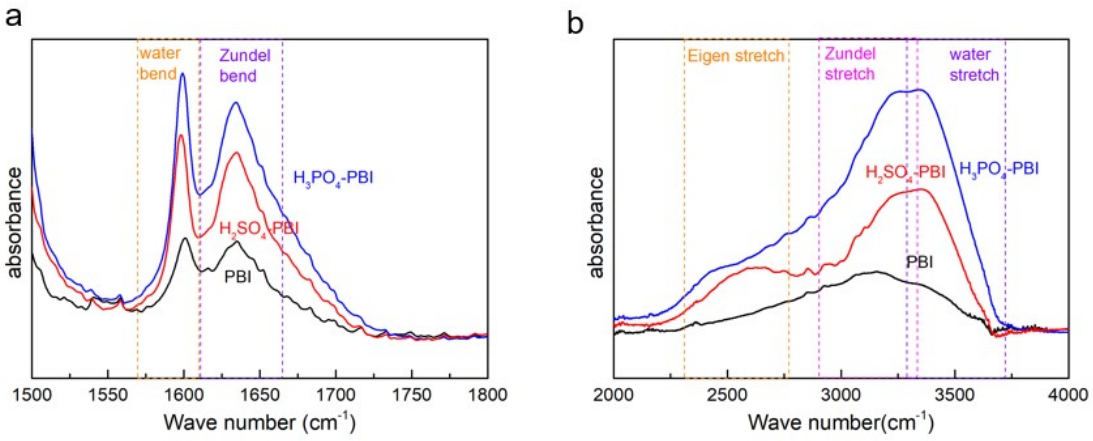

Fig. S12. The FT-IR difference spectrum between wet and dry membranes.

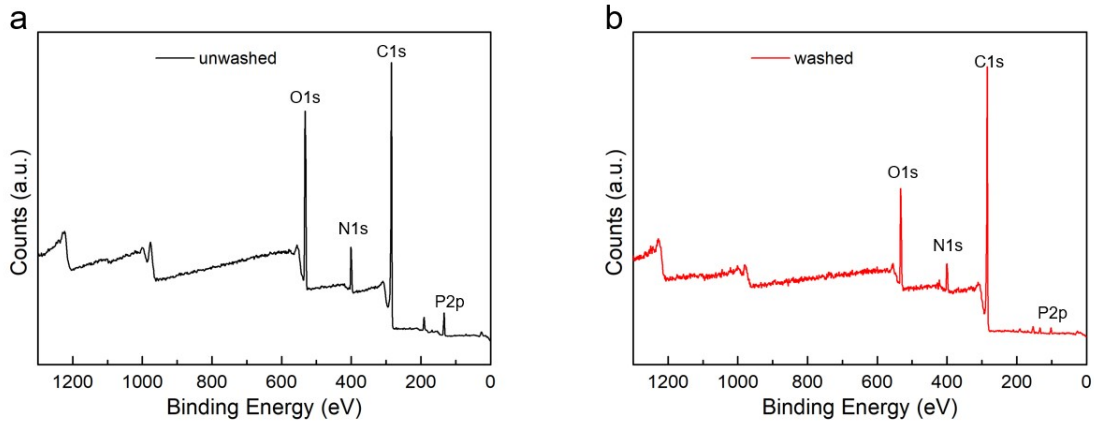

Fig. S13. The XPS survey spectrum of unwashed H_3PO_4-PBI and washed H_3PO_4-PBI.

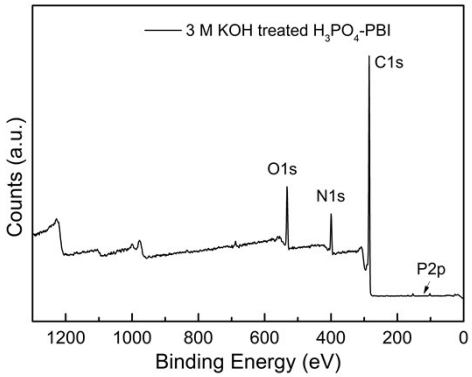

Fig. S14 The XPS survey spectrum of 3 M KOH treated H_3PO_4-PBI.

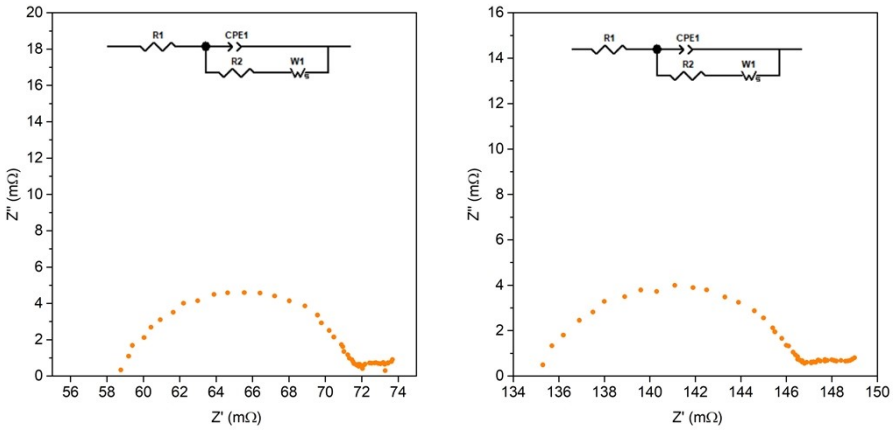

Fig. S15 The EISs of 3×3 cm^2 VFBs assembled with H_3PO_4-PBI (left) and H_2SO_4-PBI (right) at 70% SOC. Insert shows the equivalent circuit model. The ohmic resistance (R1) and charge transfer impedance (R2) are 59 mΩ and 12 mΩ for the VFB assembled with H_3PO_4-PBI, respectively; and 135 mΩ and 11 mΩ for the VFB assembled with H_2SO_4-PBI, respectively.

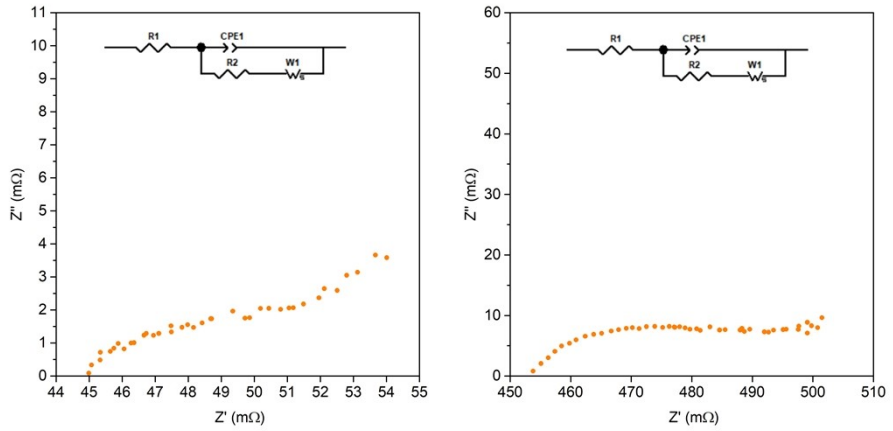

Fig. S16 The EISs of 3×3 cm^2 Alkaline Zn-Fe flow batteries assembled with H_3PO_4-PBI (left) and 3 M KOH-PBI (right) at 70% SOC. Insert shows the equivalent circuit model. The ohmic resistance (R1) are 45 mΩ and 454 mΩ for batteries assembled with H_3PO_4-PBI and 3 M KOH-PBI membranes, respectively; The charge transfer resistance (R2) is at the order of magnitude of 10^{-6} mΩ for the two batteries because of the very fast electrochemical kinetics, thus it can be neglected.

Table S1. The N1s binding energy of different PBI membranes.

	3M KOH-PBI	5.5M KOH-PBI	PBI	3M KOH-PBI-3M H_2SO_4	H_2SO_4-PBI	H_3PO_4-PBI
Pyrrole N	400.25	400.14	400.46	400.83	400.76	400.63
Pyridine N	398.44	398.43	398.33	399.3	399.49	398.68

Table S2. The atom content of washed, unwashed and 3 M KOH treated H_3PO_4-PBI measured by XPS.

Atomic (%)	C	N	O	P	P/N
Unwashed-H_3PO_4-PBI	67.14	8.15	20.70	4.02	0.49
Washed-H_3PO_4-PBI	77.14	7.41	14.02	1.42	0.19
3 M KOH treated H_3PO_4-PBI	78.57	10.80	9.78	0.47	0.05

References

1 Z. Yuan, Y. Duan, H. Zhang, X. Li, H. Zhang and I. Vankelecom, *Energy Environ. Sci.*, 2016, **9**, 441–447.

2 T. Sata, *Ion Exchange Membranes: Preparation, Characterization, Modification and Application*, Royal Society of Chemistry, 2007.

3 L. Mogg, S. Zhang, G.-P. Hao, K. Gopinadhan, D. Barry, B. L. Liu, H. M. Cheng, A. K. Geim and M. Lozada-Hidalgo, *Nat Commun*, 2019, **10**, 1–5.

4 X. Zhou, Z. Wang, R. Epsztein, C. Zhan, W. Li, J. D. Fortner, T. A. Pham, J.-H. Kim and M. Elimelech, *Science Advances*, 2020, **6**, eabd9045.

5 X. Li, H. Zhang, Z. Mai, H. Zhang and I. Vankelecom, *Energy Environ. Sci.*, 2011, **4**, 1147.

6 Q. Dai, Z. Zhao, M. Shi, C. Deng, H. Zhang and X. Li, *J. Membr. Sci.*, 2021, **632**, 119355.

7 H.-C. Yeh, M. Wang, C.-C. Chang and R.-J. Yang, *Isr. J. Chem.*, 2014, **54**, 1533–1555.